CONDENSED MATTER PHYSICS

Wigner solid pinning modes tuned by fractional quantum Hall states of a nearby layer

A. T. Hatke[1], H. Deng[2], Yang Liu[2], L. W. Engel[1]*, L. N. Pfeiffer[2], K. W. West[2], K. W. Baldwin[2], M. Shayegan[2]

We studied a bilayer system hosting two-dimensional electron systems (2DESs) in close proximity but isolated from one another by a thin barrier. One 2DES has low electron density and forms a Wigner solid (WS) at high magnetic fields. The other has much higher density and, in the same field, exhibits fractional quantum Hall states (FQHSs). The WS spectrum has resonances which are understood as pinning modes, oscillations of the WS within the residual disorder. We found the pinning mode frequencies of the WS are strongly affected by the FQHSs in the nearby layer. Analysis of the spectra indicates that the majority layer screens like a dielectric medium even when its Landau filling is $\sim 1/2$, at which the layer is essentially a composite fermion (CF) metal. Although the majority layer is only $\sim$ one WS lattice constant away, a WS site only induces an image charge of $\sim 0.1e$ in the CF metal.

INTRODUCTION

Wigner solids (WSs) occur when an electron-electron interaction dominates the zero-point or thermal motion of the carriers. They can be accessed in extremely dilute systems in the absence of a magnetic field or in a high magnetic field (B) at sufficiently low Landau level filling, ν, near the termination of the fractional quantum Hall state (FQHS) series, where WSs have long been expected (1–3). The magnetic field–induced WS in a two-dimensional electron system (2DES) is of great interest and has been studied experimentally by a variety of different techniques, including pinning mode spectroscopy (4–10), photoluminescence (11), transport (12–15), nuclear magnetic resonance (16), and time-dependent tunneling (17). As a state stabilized by electron-electron interactions, it can be expected that a WS is strongly affected by nearby screening layers or its dielectric environment. There are theoretical works (18, 19) concerning the phase diagram of a 2DES in the presence of a nearby metal gate, for which the gate carries image charges that render electron-electron interactions dipolar at distances exceeding the gate separation. For a WS near a higher–dielectric constant substrate, the screening is less strong, and the magnitude of an image charge is less than $|e|$, as was studied (18, 20) for electrons separated from these substrates by thin He films.

Through pinning mode measurements (4–10), we study here a quantum 2D WS screened by a 2DES with a much larger density in a neighboring quantum well (QW). Previous dc-transport studies (15) of such density-asymmetric double wells have demonstrated the existence of a triangular-lattice WS in close proximity to a majority layer comprising a composite fermion (CF) (21) metal, by means of geometric resonance oscillations of the CFs acted on by the WS. Our work considers the reverse and examines the effect of the CF metal and majority-layer FQHSs on the statics and pinning-mode dynamics of the WS.

We find pinning modes signifying the presence of a WS both when the majority layer is a CF metal and when it is in a gapped FQHS. The difference between the pinning modes in the presence of these majority-layer states is remarkably slight. Even for a majority-layer CF metal, screening is closest to that expected from a dielectric substrate rather than that of a nearby metal gate, and we show that such screening can be modeled by image charges of only around 10% of a WS site charge, as illustrated in Fig. 1. This result is unexpected because the CF metal and solid are so close together, only about one lattice constant of the solid away. If a normal metal were at that distance, then the WS would be drastically different than one that is in the presence of a nearly inert, gapped FQHS at low temperature; instead, we find that the $2/3$ FQHS and the CF metal have pinning mode frequencies different by at most $\sim 10\%$. The finding is even more surprising in light of the geometric resonance results (15), which show that trajectories of CFs are substantially modified by the presence of a WS.

Experimental setup

Our samples contain two 30-nm-wide GaAs QWs separated by a 10-nm-thick, undoped barrier layer of $Al_{0.24}Ga_{0.76}As$, giving a center-to-center separation of 40nm. The QWs are modulation-doped with Si δ layers asymmetrically: The bottom and top spacer layer thicknesses are 300 and 80nm, respectively. This asymmetry leads to the different 2D electron densities in the QWs. As cooled, the densities of the top, high-density layer and the bottom, low-density layer are $n_H \sim 15$ and $n_L \sim 5.0$, in units of $10^{10} cm^{-2}$, which will be used for brevity in the rest of the paper. A bottom gate is used to control n_L. As detailed in the Supplementary Materials, we obtained n_H and n_L following the procedure of Deng et al. (15, 22), adapted for microwave conductivity measurements using the setup in Fig. 1D. B-dependent charge transfer between layers for samples like ours is possible and occurs mainly for $\nu_H > 1$. To account for this, the total density (n_{tot}), which does not change with B, is obtained from low-B Shubnikov–de Haas oscillations, n_H comes from high-B majority-layer FQHS positions, and n_L in the B range of interest is found by taking the difference between n_{tot} and n_H.

RESULTS

The main result of this paper is illustrated in Fig. 2, which shows pinning modes exhibited by the WS in the minority layer, as B and hence the majority-layer filling, ν_H, are varied. The notable feature is that, although the WS resides in the minority layer, the pinning modes are clearly responding to the FQHSs of the majority layer, whose filling ν_H is marked at the right side in the figure. The pinning mode

[1]National High Magnetic Field Laboratory, Tallahassee, FL 32310, USA. [2]Department of Electrical Engineering, Princeton University, Princeton, NJ 08544, USA.
*Corresponding author. Email: engel@magnet.fsu.edu
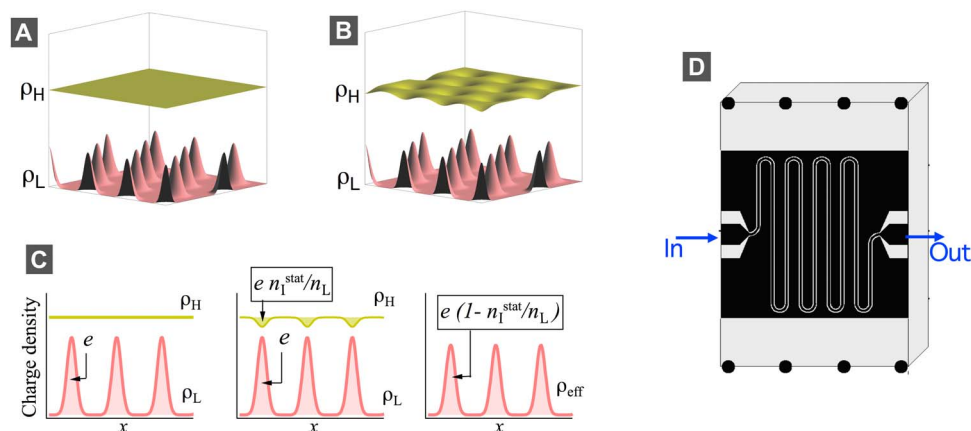
Fig. 1. WS close to CF Fermi sea. The bilayer system has a high-density (majority) top layer that hosts a CF Fermi sea when its Landau filling ν_H is around $^1/_2$ and exhibits FQHSs at odd-denominator fillings. The low-density (minority) bottom layer has a much smaller density compared to the majority layer and forms a WS when the majority layer is in the regime of FQHSs. (**A** to **C**) Schematic sketches of local charge densities of the minority layer and majority layer, $\rho_L(x, y)$ and $\rho_H(x, y)$, respectively. (A) Charge densities without screening by the majority layer. ρ_L shows the characteristic triangular Wigner lattice, but ρ_H remains uniform, as in an incompressible liquid state. (B) Same as in (A), but now, the majority-layer density screens the WS and develops dimples, regions of locally reduced charge density, which act as opposite-signed "image" charges. (C) Three panels show cuts of (A) and (B), through a line of WS electrons of charge e. The left panel is the incompressible–majority layer situation as in (A). The middle panel shows the static dielectric response of a compressible majority layer to the WS of the minority layer. The dimples, each with charge $-en_i^{stat}/n_L$, develop in the majority layer, where n_L is the areal density of minority-layer electrons, and en_i^{stat} is the image charge density. The right panel illustrates our model of the screened WS: The charge of the image is modeled as summing with the charge at its WS lattice site, creating an effective WS charge per site of $(n_L - n_i^{stat})e/n_L$. (**D**) Schematic of the sample used for microwave spectroscopy of WS pinning modes. The dark area is a metal-film coplanar waveguide (CPW) transmission line through which microwaves are propagated. The CPW has a driven center conductor and grounded side planes and is capacitively coupled to the electrons in QWs. A backgate on the bottom of the sample allows the minority-layer density to be varied.

is clearly affected by the majority-layer state but, even in the presence of the CF metal at $\nu_H \sim {}^1/_2$, remains strong. The effect of the majority-layer state on the pinning modes makes it clear that screening of the WS is present. Throughout the measurement range, the minority-layer filling $\nu_L \leq 0.113$, well within the filling-factor range of WS for high-quality, single-layer 2DESs (7, 8, 12, 14).

Figure 3A illustrates the effect of varying n_L on the pinning mode of the minority layer. $\text{Re}(\sigma_{xx})$ versus f spectra are shown at different n_L values, produced by changing backgate voltage bias. A typical characteristic of pinning modes in a single-layer WS at low ν (6, 7, 10) is that, when n_L decreases, the peak frequency f_{pk} increases, and the resonance becomes broader and weaker. We will refer to this behavior as the density effect. Its explanation in the weak-pinning theory (23–25) is that, as the WS softens at lower density, the correlation length of crystalline order in the WS decreases, and the carrier positions become more closely associated with disorder and so, on average, experience a larger restoring force due to a small displacement. The inset of Fig. 3A shows the extracted f_{pk} versus n_L. The lines are fits to $f_{pk} \propto n^{-1/2}$; this dependence has been observed previously (6, 7, 10) for single-layer samples at low densities in the low-ν WS range.
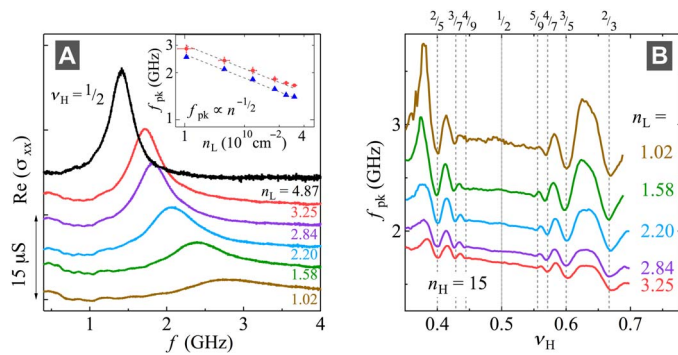
To highlight the clear response of the pinning mode to the majority-layer state, including the reduction of f_{pk} when a FQHS develops in the majority layer at its odd-denominator fillings $\nu_H = {}^2/_5, {}^3/_7, {}^4/_7, {}^3/_5$ and $^2/_3$, in Fig. 3B, we show f_{pk} as a function of ν_H for various n_L. As n_L decreases, the overall f_{pk} curves shift upward over the entire ν_H range. The oscillation amplitudes of f_{pk} seen in Fig. 3B at FQHSs of the majority layer become more pronounced when n_L decreases. This is occurring as the spacing of the minority-layer WS electrons exceeds the 40-nm interlayer separation of the double-QW structure. For example, at $n_L = 3.25$ and 1.02, the triangular WS lattice constant is $a = 60$ and 106 nm, respectively.
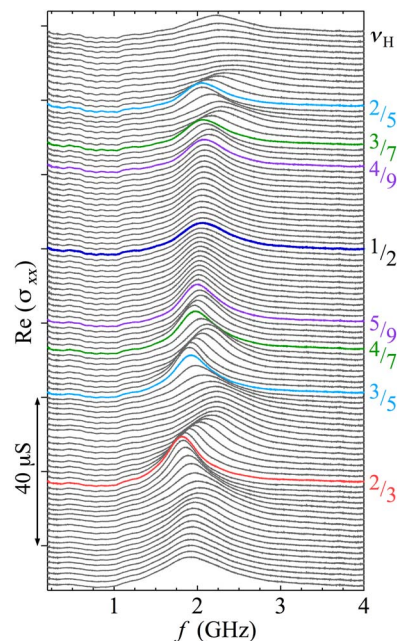
Fig. 2. Pinning mode spectra are affected by the majority layer but are present for all majority-layer states, including $\nu_H \sim {}^1/_2$. $\text{Re}(\sigma_{xx})$ versus frequency, f, spectra at many magnetic fields for majority- and minority-layer densities $n_H = 15$ and $n_L = 2.20$, respectively. Data were recorded in the low-power limit and at the bath temperature of 50 mK. Traces are vertically offset for clarity and were taken in equal steps of ν_H in the range $0.35 \leq \nu_H \leq 0.75$ ($0.053 \leq \nu_L \leq 0.113$). The majority-layer filling ν_H is labeled on the right axis.

Figure 3B shows that, for ν_H on majority-layer FQHSs, there are minima in f_{pk}. When the majority layer is in an FQHS, its ability to screen the interaction stabilizing the minority-layer WS is weakest, because the energy gap of the FQHS leaves few majority-layer charge-carrying excitations available to screen the WS. Moving ν_H away from an FQHS increases the screening due to the majority layer and reduces the correlation length of crystalline order, just as reducing the density does in the density effect, and results in a larger f_{pk}. Theories of weak pinning (23–25) all show that f_{pk} increases with larger-crystal elastic moduli.

The FQHS minima in Fig. 3B appear on top of a weak decreasing background: For each trace, the f_{pk} oscillations, and also its featureless region between 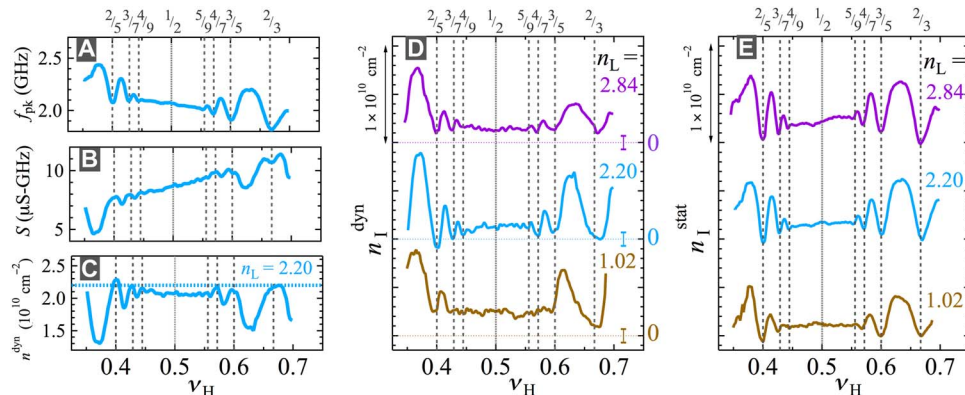$\nu_H = 0.46$ and 0.54, are superimposed on a gradual de-crease with ν_H. The decrease is similar for each trace, hence insensitive to n_L. In light of this insensitivity, we ascribe the decreasing background to effects intrinsic to the minority layer. For example, these effects could be a change in the WS stiffness (3) or a change in the disorder coupling (23–25) due to a change in the magnetic length (size of the carrier). Single-layer WSs are known to show weak dependence of f_{pk} on B over wide ranges of Landau filling (7).

DISCUSSION

Our interpretation of the data relies on the illustration in Fig. 1, in which, above the pinned WS lattice sites in the minority layer, the majority-layer local charge density develops "image" charge minima. The amount of charge in each image depends on the static dielectric response of the majority layer, not on its conductivity. The ability of the image charge to follow the WS site charge dynamically as the pinning mode is driven, on the other hand, depends on the local conductivity of the majority layer as well. At each WS lattice site, there is then a combination of an image charge with the corresponding charge in the WS. This combined object has a dipole moment, but because of the finite majority-layer local compressibility, it can also have a non-zero charge. We will characterize our pinning mode data in terms of charge densities. n^{stat} denotes the static charge density of the combined charges, and n^{dyn} denotes the (dynamic) areal charge density that moves as the pinning mode is driven. Like n_L, n^{stat} and n^{dyn} are given in units of 10^{10} cm^{-2}.

By means of the pinning mode sum rule (26), $n^{dyn} = (2B/\pi e)(S/f_{pk})$, where S is the integrated Re(σ_{xx}) versus frequency, f, for the resonance. Figure 4 (A to C) shows, for $n_L = 2.20$, how n^{dyn} is determined: f_{pk} versus ν_H in Fig. 4A and S in Fig. 4B produce n^{dyn} in Fig. 4C by use of the sum rule. S tends to increase as f_{pk} decreases and vice versa. S is increased near the majority-layer FQHSs, reflecting a lack of available cancelling image charge at these low-compressibility states. In Fig. 4C, near the peaks at the most developed FQHSs ($\nu_H = {}^2/_3$ and ${}^2/_5$), n^{dyn} approaches n_L, which is shown as a horizontal line. The difference of n_L and n^{dyn} is the image charge density in the majority layer that is moving along with the electrons of the WS, reducing the total current driven by

Fig. 3. Pinning mode as minority-layer electron density, n_L, is varied. (**A**) Re(σ_{xx}) versus f spectra at fixed $\nu_H = {}^1/_2$ ($n_H = 15$) at different n_L values. Traces are offset vertically for clarity. The density effect, typical for pinning modes, is evident as decreasing n_L increases f_{pk}, while the resonance amplitude decreases and the resonance broadens. Inset: Extracted f_{pk} versus n_L, on a log-log scale, at $\nu_H = {}^1/_2$ (circles) and ${}^2/_3$ (triangles). Dashed lines are fits to $f_{pk} \propto n_L^{-1/2}$. (**B**) f_{pk} versus ν_H at $n_H = 15$ and different n_L; traces not vertically offset. Vertical dashed lines mark rational fractional fillings (ν_H) of FQHSs. The vertical dotted line marks $\nu_H = {}^1/_2$. The upward overall increase of f_{pk} for each step down in n_L is accompanied by the oscillations of f_{pk} versus ν_H, with minima at majority-layer FQHSs.

Fig. 4. Effective WS density and image charge densities. (**A** to **C**) Plots of several quantities versus ν_H for $n_L = 2.20$, to illustrate the determination of the dynamic exffective WS density n^{dyn}: (A) shows f_{pk}, and (B) shows S and the integrated Re[σ_{xx}] versus f, and (C) shows n^{dyn} deduced from the pinning-mode sum rule $n^{dyn} = (2B/\pi e)(S/f_{pk})$. The overall downward or upward drifts respectively in f_{pk} and S versus ν_H are removed in (C), and a comparatively flat n^{dyn} versus ν_H is observed, in which the FQHSs appear as peaks. (**D**) Density, $n_l^{dyn} = (n_L - n^{dyn})$, of the image charge that moves as the pinning resonance is excited, for three n_L values, plotted versus ν_H. The data are offset for clarity, and the respective zeroes of the traces are shown as lines with error bars. (**E**) Variation of the static image charge density, n_l^{stat}, with ν_H. Traces are offset for clarity.

the resonance. We call ($n_L - n^{dyn}$) the dynamic image charge density, n_I^{dyn}. It is graphed versus ν_H for $n_L = 1.02, 2.20$ and 2.84 in Fig. 3D. n_I^{dyn} shows minima at the majority-layer FQHSs, reflecting their small compressibility and small conductivity.

The static image charge density n_I^{stat}, obtained as ($n_L - n^{stat}$), is of particular interest because of its sensitivity to the dielectric response of the majority layer without the influence of the conductivity. It is plotted in Fig. 4E. While there is no direct method to measure n^{stat} or n_I^{stat}, we can estimate their variations as ν_H sweeps through the FQHSs of the majority layer. We obtain n^{stat} independently of n^{dyn}, from the f_{pk} data of Fig. 3B alone. This is possible because in weak-pinning theories (23–25), f_{pk} is solely determined by the stiffness of the WS and the disorder acting on it. Increasing the density of a WS raises its stiffness. As described in the Supplementary Materials, the density-effect law, $f_{pk} \propto n_L^{-1/2}$, is inverted to find n_I^{stat} to within an additive constant. By obtaining n^{stat} from the density-effect law, we are treating n^{stat} as if the image charge were on the same layer as the WS; because there is an interlayer separation on the order of the WS lattice constant, this may slightly overestimate the effect of n_I^{stat} so that the n_I^{stat} that we obtain is a lower-limit estimate of the true image charge density. Neglecting the finite compressibility of the majority layer at $\nu = 2/3$ and taking $n_I^{stat}(\nu_H = 2/3) = 0$, we find that this low-estimate $n_I^{stat}(\nu_H = 1/2)$ is about 10% of n_L for the three n_L values of Fig. 4: 1.02, 2.20, and 2.84. Overall, we find the variations of n_I^{stat} and n_I^{dyn} to be of similar size for most ν_H values. This implies that the image charge in the majority layer moves with the WS as the resonance is driven.

This estimated $n_I^{stat}(\nu_H = 1/2)$ is in rough agreement with estimates of $n_I^{dyn}(\nu_H = 1/2)$, which are on the order of their error, about 10% of n_L as well. It is unexpected that FQHSs at $\nu_H = 2/3$ and $2/5$ at a temperature well below their energy gaps have image charge densities so close to those at $\nu_H = 1/2$ at which the majority-layer state is well described by a CF metal. If the CF metal were able to respond to a WS site with image charges equal to an electronic charge, as one might expect, the pinning mode for $\nu_H \sim 1/2$ would be much more strongly affected than that observed here and might not even be present. Thus, the CF metal is remarkably inefficient at screening. Figure 4 (B and C) shows that the image charge density, hence the screening, is far larger in the transition regions between the FQHSs, where it is expected that there is a network of edge states that can respond to the WS charge (27).

In summary, we study a WS separated from FQHSs by a distance comparable to its lattice constant. We observe a pinning mode from the minority-layer WS, indicating its existence even in the presence of the nearby, screening majority layer. The pinning mode is strongly affected by the majority-layer FQHSs, exhibiting a reduction in f_{pk} with an increase in S around FQHSs. We find that these phenomena can be modeled by considering image charges in the majority layer and regarding them as reducing the WS charge. The image charge is assessed to be only about 10% of the WS charge even near $\nu_H = 1/2$. It is substantially larger at the transitions between FQHSs. Comparing static and dynamic estimates of image charge indicates that, in large part, the image charge oscillates as the pinning mode is driven.

METHODS

We performed microwave spectroscopy (6–10) using a coplanar waveguide (CPW) patterned in a Cr:Au film on the top surface of the sample. A top view schematic of the measurement is shown in Fig. 1D. We calculate the diagonal conductivity as $\sigma_{xx}(f) = (s/lZ_0)\ln(t/t_0)$, where $s = 30$ μm is the distance between the center conductor and ground plane, $l = 28$ mm is the length of the CPW, $Z_0 = 50$ ohm is the characteristic impedance without the 2DES, t is the transmitted signal amplitude, and t_0 is the normalizing amplitude. The microwave measurements were carried out in the low-power limit, such that the results were not sensitive to the excitation power at our bath temperature of $T = 50$ mK.

REFERENCES AND NOTES

1. Y. E. Lozovik, V. Yudson, Crystallisation of a two dimensional electron gas in magnetic field. *JETP Lett.* **22**, 11–12 (1975).
2. K. Yang, F. D. M. Haldane, E. H. Rezayi, Wigner crystals in the lowest Landau level at low-filling factors. *Phys. Rev. B* **64**, 081301 (2001).
3. J.-W. Rhim, J. K. Jain, K. Park, Analytical theory of strongly correlated Wigner crystals in the lowest Landau level. *Phys. Rev. B* **92**, 121103 (2015).
4. E. Y. Andrei, G. Deville, D. C. Glattli, F. I. B. Williams, E. Paris, B. Etienne, Observation of a magnetically induced Wigner solid. *Phys. Rev. Lett.* **60**, 2765–2768 (1988).
5. F. I. B. Williams, P. A. Wright, R. G. Clark, E. Y. Andrei, G. Deville, D. C. Glattli, O. Probst, B. Etienne, C. Dorin, C. T. Foxon, J. J. Harris, Conduction threshold and pinning frequency of magnetically induced Wigner solid. *Phys. Rev. Lett.* **66**, 3285–3288 (1991).
6. C.-C. Li, J. Yoon, L. W. Engel, D. Shahar, D. C. Tsui, M. Shayegan, Microwave resonance and weak pinning in two-dimensional hole systems at high magnetic fields. *Phys. Rev. B* **61**, 10905–10909 (2000).
7. P. D. Ye, L. W. Engel, D. C. Tsui, R. M. Lewis, L. N. Pfeiffer, K. W. West, Correlation lengths of the Wigner-crystal order in a two-dimensional electron system at high magnetic fields. *Phys. Rev. Lett.* **89**, 176802 (2002).
8. Y. P. Chen, R. M. Lewis, L. W. Engel, D. C. Tsui, P. D. Ye, Z. H. Wang, L. N. Pfeiffer, K. W. West, Evidence for two different solid phases of two-dimensional electrons in high magnetic fields. *Phys. Rev. Lett.* **93**, 206805 (2004).
9. G. Sambandamurthy, Z. Wang, R. M. Lewis, Y. P. Chen, L. W. Engel, D. C. Tsui, L. N. Pfeiffer, K. W. West, Pinning mode resonances of new phases of 2D electron systems in high magnetic fields. *Solid State Commun.* **140**, 100–106 (2006).
10. Z. Wang, Y. P. Chen, H. Zhu, L. W. Engel, D. C. Tsui, E. Tutuc, M. Shayegan, Unequal layer densities in bilayer Wigner crystal at high magnetic fields. *Phys. Rev. B* **85**, 195408 (2012).
11. I. V. Kukushkin, V. I. Fal'ko, R. J. Haug, K. von Klitzing, K. Eberl, K. Tötemayer, Evidence of the triangular lattice of crystallized electrons from time resolved luminescence. *Phys. Rev. Lett.* **72**, 3594–3597 (1994).
12. H. W. Jiang, R. L. Willett, H. L. Stormer, D. C. Tsui, L. N. Pfeiffer, K. W. West, Quantum liquid versus electron solid around ν=1/5 Landau-level filling. *Phys. Rev. Lett.* **65**, 633–636 (1990).
13. V. J. Goldman, M. Santos, M. Shayegan, J. E. Cunningham, Evidence for two-dimensional quantum Wigner crystal. *Phys. Rev. Lett.* **65**, 2189–2192 (1990).
14. M. Shayegan, in *Perspectives in Quantum Hall Effects*, S. Das Sarma, A. Pinczuk, Eds. (Wiley-Interscience, 1997), p. 343.
15. H. Deng, Y. Liu, I. Jo, L. N. Pfeiffer, K. W. West, K. W. Baldwin, M. Shayegan, Commensurability oscillations of composite fermions induced by the periodic potential of a Wigner crystal. *Phys. Rev. Lett.* **117**, 096601 (2016).
16. L. Tiemann, T. D. Rhone, N. Shibata, K. Muraki, NMR profiling of quantum electron solids in high magnetic fields. *Nat. Phys.* **10**, 648–652 (2014).
17. J. Jang, B. M. Hunt, L. N. Pfeiffer, K. W. West, R. C. Ashoori, Sharp tunnelling resonance from the vibrations of an electronic Wigner crystal. *Nat. Phys.* **13**, 340–344 (2017).
18. F. M. Peeters, Two-dimensional Wigner crystal of electrons on a helium film: Static and dynamical properties. *Phys. Rev. B* **30**, 159–165 (1984).

19. B. Spivak, S. A. Kivelson, Phases intermediate between a two-dimensional electron liquid and Wigner crystal. *Phys. Rev. B* **70**, 155114 (2004).

20. G. Mistura, T. Günzler, S. Neser, P. Leiderer, Microwave study of screened two-dimensional electron crystals on helium films. *Phys. Rev. B* **56**, 8360–8366 (1997).

21. J. K. Jain, *Composite Fermions* (Cambridge Univ. Press, 2007).

22. H. Deng, Y. Liu, I. Jo, L. N. Pfeiffer, K. W. West, K. W. Baldwin, M. Shayegan, Interaction-induced interlayer charge transfer in the extreme quantum limit. *Phys. Rev. B* **96**, 081102 (2017).

23. R. Chitra, T. Giamarchi, P. Le Doussal, Pinned Wigner crystals. *Phys. Rev. B* **65**, 035312 (2001).

24. H. A. Fertig, Electromagnetic response of a pinned Wigner crystal. *Phys. Rev. B* **59**, 2120–2141 (1999).

25. M. M. Fogler, D. A. Huse, Dynamical response of a pinned two-dimensional Wigner crystal. *Phys. Rev. B* **62**, 7553–7570 (2000).

26. H. Fukuyama, P. A. Lee, Pinning and conductivity of two-dimensional charge-density waves in magnetic fields. *Phys. Rev. B* **18**, 6245–6252 (1978).

27. J. Martin, S. Ilani, B. Verdene, J. Smet, V. Umansky, D. Mahalu, D. Schuh, G. Abstreiter, A. Yacoby, Localization of fractionally charged quasi-particles. *Science* **305**, 980–983 (2004).

28. J. P. Eisenstein, L. N. Pfeiffer, K. W. West, Compressibility of the two-dimensional electron gas: Measurements of the zero-field exchange energy and fractional quantum Hall gap. *Phys. Rev. B* **50**, 1760–1778 (1994).

29. G. Fano, F. Ortolani, Interpolation formula for the energy of a two-dimensional electron gas in the lowest Landau level. *Phys. Rev. B* **37**, 8179–8181 (1988).

Citation: A. T. Hatke, H. Deng, Y. Liu, L. W. Engel, L. N. Pfeiffer, K. W. West, K. W. Baldwin, M. Shayegan, Wigner solid pinning modes tuned by fractional quantum Hall states of a nearby layer. *Sci. Adv.* **5**, eaao2848 (2019).